Graphical Abstract

Single droplet drying of whey protein dispersions

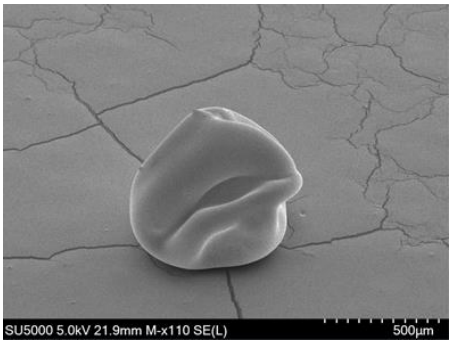

Soluble whey protein aggregate particle
Initial colloidal size = 50 nm

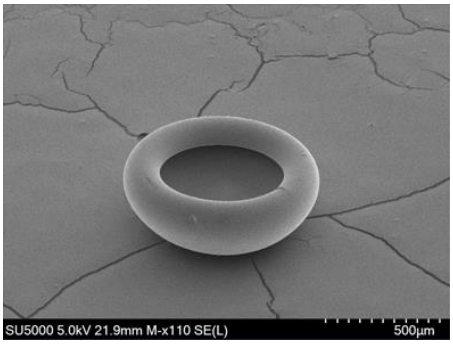

Fractal whey protein microgel particle
Initial colloidal size = 300 nm

Morphology development in single drop drying for native and aggregated whey protein dispersions

L. Malafronte*[1], D. Ruoff[1], D. Z. Gunes[2], F. Lequeux[3], C. Schmitt[2], E. J. Windhab[1]

1 Laboratory of Food Process Engineering, Institute of Food, Nutrition and Health, ETH Zurich, LFO E18 Schmelzbergstrasse 9, CH-8092 Zurich, Switzerland

2 Nestlé Research, Nestlé Institute of Material Sciences, Vers-chez-les-Blanc, CH-1000 Lausanne 26, Switzerland

3 Laboratoire Sciences et Ingénierie de la Matière Molle, CNRS, ESPCI Paris, PSL Research University, 10 rue Vauquelin, Paris, France

**loredanamalafronte@gmail.com*

Abstract

Native and aggregated whey proteins (WP) are used in food and pharmaceutical applications as stabilizers, thickeners and carriers. For increasing shelf-life and facilitating transportation, WP are transformed into powders by spray-drying. Powder functional properties strongly depend on the final particle morphology. Focusing on colloidal aspects of drying, the goal of this work is to: (i) investigate morphology development during single drop drying of native and aggregated whey protein dispersions; (ii) use structure-mechanical parameters to predict the final morphology. Results showed evaporation rate and morphology development characteristic times are not affected significantly by colloidal size. However, the final morphology of particles depends on WP colloidal size. For small colloids, particles are shriveled, while their shape is cup-like for larger colloids. Structure–mechanical parameters allowed predicting a buckled/shriveled morphology in agreement with experimental observations. Specifically, predictions anticipated the formation of a solid shell at the particle surface, which is compressed during drying, as a result of colloidal interactions being dominated by van der Waals forces. This work provides a rationalization of morphology development of WP particles. In addition, the work suggests that the elastic – or gel – formation, that is governed by the permeation, may be very different depending on the permeability of the proteins gel. The collapse from a dispersion to an elastic gel may be responsible for the shriveled to buckled transition. The work shows that diverse final morphologies can be achieved using same drying conditions and composition, while only changing the degree of colloidal aggregation.

1.1 Introduction

The control of particle morphology during the spray drying of food powders is one of the key factors affecting powder properties in food applications, under dry and reconstituted states. The dry powder properties include powder density, porosity, pore size distribution and flowability. The reconstituted powder properties are decided based on the target final product properties. They depend on particle size distribution, the particle structure, as well as the wetting and re-dispersion properties, which can follow complex mechanisms. This is true in particular for dairy based powders [1], [2], [3], which are the most common powder in the food industry. Typical dairy based powders are skim and whole milk, high fat and whey protein powders. They are used for preparation of instant drinks, or as ingredients i.e. in cheese, chocolate and baking products [4]. Reconstitution of dairy based powders is a slow and complex mechanism [5], [6]. Recent works showed that full powder reconstitution may be slower than usually described, and indeed depends on the drying conditions – whereby particulate structures can take up to over an hour to fully re-disperse and dissolve. Crowley et al. [7] showed that the lactose to protein ratio strongly influences particle morphology, while low lactose concentration was shown to imply buckled particle or vacuole type morphologies, along with slower dissolution. Final particle morphology depends also on protein composition. Sadek et al. [8] and Lanotte et al. [9] demonstrated that whey protein particles are spherical and hollow, native casein particles are shriveled, and protein

mixtures leads to hybrid particle morphologies. In addition to this, Fang et al. [10] showed the drying rate as a critical factor affecting particle morphology. The goal of the present work is to attempt rationalizing the behavior of well-defined dispersions of protein aggregates in their single drop drying behavior: drying rate, kinetics and type of morphologies developing. The reference system is a solution of non-aggregated whey protein, and the aggregate size and morphologies are varied. Whey protein and their aggregate has been selected as reference system since they are of great interest for food application, especially for their emulsifying capacity [11], [12], [13].

Generic research in the field of colloid suspension drying revealed the key mechanisms in play for systems whose behavior may be modeled with a few parameters describing colloidal interactions, Brownian motion, evaporation rate, as well as hydrodynamic stresses generated during drying. It was established from experiments using model colloidal suspensions, that the Péclet number, which balances the diffusion time of the colloidal particle (or molecule) over a characteristic distance with the drying time, is a key parameter for describing the drying mechanism. Under conditions of fast drying i.e. large Péclet number, the drop shrinkage is so fast that Brownian motion does not keep the colloids well dispersed within the drop, so they accumulate near the drop surface in the form of a concentrated suspension, forming a shell with solid mechanical properties. Depending on whether colloidal gelation occurred over nearly the whole drop volume before a solid shell could form or not, buckling will occur or not. Lintingre et al. [14] described in detail the dimensionless parameters, which allow for predicting the Péclet range for shell formation, as well as the conditions for buckling. It is known that aggregation can occur in the particle shell, even under conditions of colloidal interactions, which would be repulsive in the absence of a drying mechanism. The conditions of buckling are usually reached earlier for weaker repulsion or slight attraction between colloids, while strong attraction may lead to drop gelation and resistance to buckling.

1.2 Background

During drying, colloidal particles accumulate at the droplet-air interface, creating a solid shell that may buckle, leading to non-spherical morphologies. Such a phenomenon is explained by calculating relevant parameters as suggested by Lintingre et al. [14], such as the Péclet dimensionless number, Pe, associated to the dispersed particles, the critical buckling pressure, P_{buck}, the capillary pressure, P_{cap}, the Darcy's pressure, P_{Darcy}, and the Derjaguin Landau Verwey Overbeek (DLVO) potential, V_{DLVO}.

Pe is used to compare the effect of colloidal diffusion and drying rate (detailed assumptions available in [14]):

$$Pe = \frac{R^2}{\tau_{dry}} \frac{6\pi\eta a}{kT} = m \frac{6\pi\eta a}{kT} \quad \text{(Eq. 1)}$$

Where k is Boltzman's constant, T is the drying temperature, η is the solvent viscosity, a is the colloidal particle radius, τ_{dry}, is the drying time, R is the radius of the droplet (all in S.I. units). The constant m is introduced above and is equal to R^2 / τ_{dry}, namely evaporation rate.

If the Péclet number is larger than 1, the particles will accumulate and form a shell. Under the Darcy pressure, this shell may become an elastic solid. This is often called sol-gel transition and may lead to fracture on macroscopic sample [15]. The particles forms an elastic – gel-like – shell, because the solvent continue to evaporate, the volume of liquid enclosed in the shell will decrease. Consequently, the shell will buckle, if the pressure in the shell exceed a critical value.

P_{buck} is the critical pressure above which the shell buckles and collapses:

$$P_{buck} = 2E\left(\frac{h}{R}\right)^2 \sqrt{3(1-\nu^2)} \quad \text{(Eq. 2)}$$

E denotes the shell's Young modulus, v is the Poisson ratio, h is its thickness. If the shell forms progressively, its thickness will increase with time. Since P_{buck} increases with the square of h, buckling will appear for very small h, as soon as the shell can be considered as an elastic body. It is a reasonable estimate to assume that the minimum value of h is 5a, meaning 5 layers of particles are needed to consider that the shell is a solid body. In contrast, if the shell forms instantaneously, the thickness h may be large at the onset of the elastic body formation and equal to R/5 where R is the droplet radius for the shell thickness to occur. Above this thickness, no buckling will occur and a hollow sphere will be obtained.

The pressure exerted on the shell by the liquid inside is limited only by the water flow through the porous shell and thus by the capillary pressure, P_{cap}, which is maximum before penetration of air into the shell [16]:

$$P_{cap} \approx \frac{4\gamma}{d} \quad \text{(Eq. 3)}$$

Where γ is the droplet-air interfacial tension and d the pore diameter.

The formation of the shell itself is driven by the water gradient pressure across the shell, namely Darcy's pressure. P_{Darcy} brings together the colloidal particles promoting aggregation:

$$P_{Darcy} = \frac{\eta v}{k_p} h \quad \text{(Eq. 4)}$$

Where v is the relative velocity between liquid and particle shell, $v \approx R/\tau_{dry}$, k_p the shell permeability calculated as a function of the packing volume fraction and based on the Karman Cozeny expression, Φ_c, as:

$$k_p = \frac{a^2(1-\Phi_c)^3}{45\Phi_c^2} \quad \text{(Eq. 5)}$$

Lastly, P_{Darcy} succeeds to from an elastic shell only if it is able to overcome the electrostatic repulsion in between colloidal particles. At small distances, this repulsion is given by the Derjaguin Landau Verwey Overbeek (DLVO) potential, V_{DLVO}, superimposing charge induced repulsion and van der Waals attraction. At colloidal particle distances r << a it is:

$$V_{DLVO}(r) = 64\pi kT\Gamma^2\rho_i\lambda_D^2 a e^{-r/\lambda_D} - \frac{Aa}{12r} \quad \text{(Eq. 6)}$$

$$\Gamma = \tanh\left(\frac{e\zeta}{4kT}\right) \quad \text{(Eq. 7)}$$

Where e is the electron charge, ζ is the surface potential, A is the Hamaker van der Waals constant, ρ_i is the ion density in the solvent (mol m^{-3}). λ_D denotes the Debye length calculated as [17]:

$$\lambda_D = \sqrt{\frac{\varepsilon\, \Re T}{2\,\rho\, F^2\, I\, b^\ominus}} \quad \text{(Eq. 8)}$$

Where ε is the dielectric constant, $\Re$ is the ideal gas constant, ρ is the density of the solution, F is the Faraday's constant, and $b^\ominus$ is the standard molality (mol kg^{-1}), I is the dimensionless ionic strength of the initial solution:

$$I = \frac{1}{2}\sum_i z_i^2 \frac{b_i}{b^\ominus} \quad \text{(Eq. 9)}$$

z_i denotes the charge number of an ion i, and b_i its molality.

Material and Methods

Materials

Whey protein isolate (WPI) powder (BiPRO, lot number LE 020-7-420) was purchased from AgroPur Inc. (Jerome, USA). This product is obtained by ionic chromatography of ultrafiltered sweet whey in order to remove caseino-glycomacropeptide and contains therefore no casein fractions [18]. According to the manufacturer, WPI powder has a composition of (in g/100g): 93.2 protein (Nx6.38), 4.4 moisture, 2.3 ash, and fat 0.5. Sodium chloride (NaCl), hydrochloride (HCl), sodium hydroxide (NaOH) were purchased from VWR, Titrisol©, Sigma-Aldrich respectively.

Preparation of protein dispersions

WPI dispersions at 4 and 7 wt% solid content, which correspond to a protein content of 3.7 and 6.5 wt%, respectively. They were prepared using Milli-Q water (Millipore Synergy UV, Millipore AG, Switzerland) in batches of 1L by stirring over night to ensure complete hydration. Three different types of WPI aggregates were produced in a double-jacketed cylindrical vessel, equipped with a turbine mixer (Janke & Kunkel RW 20, IKA Labortechnik, Germany), two water baths, one for heating and one for cooling, and a temperature controller (TM-947SD, Lutron Electronic).

The WPI aggregates were produced according to the protocol of Schmitt et al. [18] and Phan-Xuan [19]. The preparation of dispersions of WPI aggregates comprises:

(i) pH adjustment of the initial WPI dispersion by dropwise addition of 1 M HCl or NaOH under vigorous stirring, the different conditions are described in Table 1;
(ii) WPI dispersions were transferred to the cylindrical vessel, and heated under stirring (200 rpm) to 85°C in about 15 min. The temperature was held for 10 min. Dispersions were then rapidly cooled down using ice water until room temperature to stop the aggregation process.

After aggregates were produced, dispersions were diluted to the same initial solid content of 4 wt%. Dispersions with added salt were prepared right before experiments by adding NaCl in the concentration of 1 wt%, 3 wt% and 6 wt% on a dry basis (db).

Colloidal size determination

The size measurements were performed using a Zeta sizer Nano ZS dynamic light scattering device (Malvern Instruments, Worcestershire, U.K.), equipped with a He-Ne laser emitting a polarized light beam of wavelength of 633nm. For the measurements, all protein dispersions were diluted 1:1000 using Milli-Q water. WPI dispersions were filtered prior measurement using a 0.1 and a 0.025 µm filter (NC 03 Membrane Filters, Schleicher & Schuell, Germany) [20]. The measurements were performed in 10 mm disposable cuvettes at a temperature of 25°C.The scattered intensity fluctuations were collected at a backscattering angle of 173°. The results were averaged over 3 runs and the time correlation function of the scattered intensity was analyzed using the CONTIN method [21].

Single droplet drying

Drying experiments were conducted using a single droplet drying kinetics device, composed by a single axial acoustic levitator (tec5 ultrasonic levitator, Germany), which works at a standard frequency of 58 kHz. It consists of a transducer that creates an acoustic wave, and a concave reflector that reflects it back, in order to create a standing wave to allow droplet levitating (Figure 1). A free jet nozzle is integrated into the reflector; it has a diameter of 1 mm and allows dry air to be blown upward around the levitated droplet. The dry air was supplied by a compressed dry air cylinder. Measurements were performed at constant airflow of 100 cm^3min^{-1} and at room temperature (23 ± 2°C). The distance between reflector and transducer was 2 cm, and the power of the acoustic field was adjusted via HF controller to ensure droplet stability. A 2 µl bubble-free droplet was inserted into the acoustic field using a 100µl syringe (SGE, Australia). Morphological and size changes of the droplet during drying were recorded using a Nikon camera D5300 (Tokyo, Japan) together with a macro lens Nikon Micro

Nikkor, 52 mm 1:1 (Tokyo, Japan). Two light sources were used depending on whether morphology or size changes were investigated. A front light system was used to follow morphology during drying, it includes two OSRAM Parathom® Advanced GU5.3 MR16 LED lights in position A. A back light system, instead, was used to follow morphology changes, it consists of a green LED emitter (LZC-00MC40 RGB LED, LedEng Inc.) controlled by a linear RGB LED Controller in position B. The generated images were then analysed using image analysis as described in the next paragraph. All measurements were carried out in triplicates.

Evaporation rate calculation

Pictures obtained using back lighting were used to measure the size change of each droplet during the drying time using image analysis. Original images were cut into 500 x 500 pixels images and processed using the software CellProfiler 2.2.0. The image analysis pipeline consists of the following sequence of operations: Log transform (base 2), Invert, Identify Primary Objects, Measure Object Size Shape, Export to Spread Sheet. The output comprises the object area in pixels, which was converted in real size using the transducer as a reference size. Finally, the radius of the droplet was calculated and the evaporation rate could be determined using the "radius squared law"[22]:

$$r^2(t) = R_0^2 - mt \qquad \text{(Eq. 10)}$$

Where r is droplet radius as a function of the time, t; R_0 is the initial droplet radius and m the evaporation rate (all in S.I. units). The constant m is equal to R^2 / τ_{dry} as introduced above (see Eq. 1). The evaporation rate was calculated only in the first 210 s of drying, which is the period when all measurements show a linear spherical shrinkage. Initial volume of the droplets was also calculated and only droplets in the range of 2 ± 0.3 µl were used for the analysis.

Morphology characterization

Morphology changes over the drying time were investigated using pictures obtained by front lighting. Morphology was characterized by two characteristic times, locking and buckling time, identified visually as suggested by Both et al. [2]. The locking time is defined as the time when the droplet becomes non-spherical, while the buckling time is when significant morphology development is observed. Examples of locking and buckling time are reported in Figure 2.

Scanning electron microscopy

Selected dried particles were visualised with Scanning Electron Microscopy (SEM, Hitachi, SU5000). Particles were placed on carbon tape and coated with a 10 nm layer of gold (CCU-010 Metal Safematic). Images were obtained under vacuum at an accelerating voltage of 5 kV.

Results

Colloidal dispersion characterization

Three types of WPI aggregates, namely soluble whey protein aggregates (WPA), whey protein microgels (WPM) and fractal WPM, were produced according to the protocol reported previously. Using these conditions, more than 80% of the native whey proteins are converted into: microgels, fractal aggregates of microgels or soluble fractal aggregates [18, 19]. The protein fraction coexisting together with microgels is composed by soluble aggregates which are characterized by a fractal dimension of about 1.8 [19]. Additionally, a WPI dispersion was prepared. Aggregated dispersions were used with and without NaCl addition. Dispersions were characterized in terms of colloidal size and results are reported in Table 2. Results show that the four dispersions have different average colloidal sizes. WPI dispersions were characterized prior and after filtration.

The smallest colloids are WPA (49.2 nm), followed by WPI (181.2 nm), WPM (230 nm) and finally fractal WPM (290.9 nm). Colloidal size of WPA, WPM and fractal WPM are in agreement with results reported in literature. The expected range of WPA hydrodynamic diameter is from 43 to 58 nm [18], [23]. Instead, WPM and fractal WPM hydrodynamic diameters are expected in the range from 100 to 1000 nm [24], with fractal WPM being larger than WPM since they consist of WPM assembled into a self-similar structure [25]. Addition of NaCl does not modify the colloidal size of aggregated protein dispersion, since salt was added right before size and drying measurements to avoid exactly colloidal size enlargement.

The hydrodynamic diameter of WPI results to be higher than expected due to the presence of self-forming aggregates of WPI in water. The expected size was about 5-10 nm since it is composed by native proteins [26], [27], as also confirmed by filtered WPI dispersions measurements. In this study, we consider the average size of unfiltered WPI dispersions, since filtration was not performed prior drying experiments.

Single droplet drying

Single droplet of protein dispersions were dried using the acoustic levitator droplet drying device. Morphology development of a single droplet during the drying time was monitored to determine the evaporation rate, as well as the locking and buckling times.

Evaporation rate of the constant drying rate period was evaluated and results are shown in Figure 3 as a function of the colloidal diameter and added salt concentration. Ideal shrinkage occurs during the constant drying period; hence, the "radius squared law" was applied. Results show that for all dispersions, evaporation rate ranges from 4×10^{-10} to 8×10^{-10} $m^2 s^{-1}$. In case of 0 and 6 wt% (db) added salt, the evaporation rate seems to increase with the colloidal size, however, no trend can be observed in case of 1 and 3 wt% (db) added salt.

Figure 3 shows the locking and buckling time of single droplets as a function of colloidal size for no added NaCl. For all solutions, average buckling time is always higher than average locking time, except for soluble WPA, for which there is no difference between locking and buckling time. In addition to this, buckling and locking time for WPA is above 12 min, instead in case of WPI, WPM and fractal WPM they are lower than 8 min. In case of WPI, WPM and fractal WPM it seems that locking and buckling time increase as a function of the colloidal size, suggesting that shape instability could be delayed by enlarging the colloid particle. Addition of salt to WPI, WPM and fractal WPM solution does not seem to affect the locking and buckling time, except for soluble WPA (Figure 4). For soluble WPA, addition of salt seems to anticipate shape instability, especially in case of 1 wt% added NaCl.

The final morphology of single particles was observed using a macro camera and SEM (Figure 5). Soluble WPA with no added salt exhibits a shriveled morphology, whereas WPI, WPM and fractal WPM show a cup-like shape. Salt addition does not seem to affect final particle morphology of WPM and fractal WPM. In case of soluble WPA, addition of NaCl leads to the formation of a shriveled particle with a lower degree of invaginations. Hence, for small colloidal size particles are shriveled, while their shape is cup-like for larger colloids. Morphology of WPI particles are in agreement with results reported by Sadek et al [8] and Lanotte et al [9].

Shell formation and mechanical properties

In order to explain morphology development of single droplets during drying, parameters affecting shell formation and mechanical properties are estimated. Pe is calculated considering $k = 1.38 \times 10^{-23}$ J K^{-1}, T = 298 K, because drying is performed at room temperature, and $\eta = 0.001$ Pa.s, since in this case the solvent is water. The ratio R^2 / τ_{dry} is equal to the evaporation rate, m, calculated from Eq 10. P_{buck}

is estimated assuming E = 10^4 Pa [28], ν = 0.4 [29], h = 5a, R is the droplet radius at the locking time. In case of P_{cap}, γ ≈ 50 mN.m^{-1} [30] and pore diameter d = a/5. P_{Darcy} is estimated assuming a random close packing volume fraction, Φ_c = 0.64 [31], this assumption implies that no strong particulate gel forms within the shell, or at least not before the shell reaches a particle concentration around random close packing. V_{DLVO} is calculated considering e = 1.6 x 10^{-19} A s, ζ ≈ -20 mV [30], A = 10^{-20} J, ε = 7.1 10^{-10} J^{-1}C^{2}m^{-1}, R = 8.314 J K^{-1} mol^{-1}, ρ = 1000 kg m^{-3}, F = 9.65 x 10^4 C mol^{-1}. I and ρ_i are estimated as according to the following composition of the initial WPI powder: protein content of 93.6 wt%, 4.4 wt% moisture, 0.3 wt% fat, < 3 wt% lactose and 1.7 wt% ash of which 0.079 wt% Ca^{2+}, 0.006 wt% Mg^{2+}, 0.037 wt% K^+, 0.767 wt% Na^+, 0.001 wt% Cl^-)[30].

In Figure 6, Pe as a function of percentage of added salt for all dispersions is shown. In all cases Pe > 1, which indicates that particles will accumulate at the surface of the droplet creating a shell [32]. No significant effect of addition of NaCl can be observed. In case of $P_{cap} > P_{buck}$, buckling is expected as soon as the shell becomes elastic, independent of its thickness. Calculated P_{cap} and P_{buck} are shown in Figure 6 and Figure 7 respectively. P_{cap} is inversely proportional to the colloidal size as reported in Eq. 4 and it ranges from a minimum of 7 x 10^6 Pa in case of fractal WPM, to a maximum of 4 x 10^7 Pa for soluble WPA. P_{buck}, instead, results to be much lower, with a maximum value of 7 x 10^{-2} Pa. Hence, buckled/shrivelled morphologies are expected, in agreement to particle morphologies observed in this work (Figure 5). P_{Darcy} is estimated ranging from 3 x 10^5 to 2 x 10^7 Pa (Figure 7), in agreement with osmotic pressure values of protein colloids reported in literature [33]. P_{Darcy} confirms solid shell formation and indicates that accumulated colloidal particles are compressed and further aggregated. This pressure difference could be counterbalanced by charge-induced repulsions of colloidal particles, described by the DLVO potential. In this case, DLVO potential results to be always negative for all solutions, and no effect of salt addition is observed, as estimated from Eq. 6. Negative or attractive DLVO potential indicates that colloidal interaction is dominated by van der Waals attraction. The absence of effect of salt addition indicates that the amount of ions already presented in the initial powder is enough to completely screen out the electrostatic repulsion, at the concentrations worked on.

The occurrence of a different final particle morphology can now be discussed (Figure 5). In the case of buckling of droplet with a thin elastic layer, an instability with the largest wavelength mode is expected (i.e. bottom right picture in Figure 5). Instead, it is known that if an elastic layer is supported by another elastic layer, the first one being more compressed than the second, an instability may occurs with a wavelength about the thickness of the first layer [34]. Thus, the formation of a shrivelled particle (i.e. bottom left picture in Figure 5) can be explained by assuming the formation of a gel inside the droplets, which is a loose network of proteins. At the surface of the gel, a denser elastic phase is formed, because the Darcy pressure is larger near the surface (P_{Darcy} increases from the centre of the droplets toward its surface). This dense shell is compressed, because of the droplet shrinkage due to evaporation, it cannot sustain the compression and it buckles. However, the inner gel can sustain compression, since it is less dense, and acts like an elastic substrate with a low compression stress. This results in a buckling instability with a wavelength of about the dense layer thickness, leading to a shrivelled dry droplet. At opposite, in the absence of an inner gel, the wavelength selected by buckling is the largest possible and a cup-like shape particle is formed. In this study, a shrivelled morphology is observed only for particles of soluble WPA dispersions. Soluble WPA particles showed the smallest Pe number (Figure 6), indicating that diffusion is more efficient against shell formation when compared to the other protein dispersions investigated. Specifically, diffusion dominates convection at a characteristic length of the order of D/U = 2R/Pe, where U is the water velocity at droplet surface, and D the diffusion coefficient given by D = kT/6πηa (see Eq. 1). Below this length, diffusion dominates, and a homogeneous proteins layer is maintained, which becomes more and more concentrated. However, the layer collapse due to Darcy pressure. For soluble WPA this length is about 10 μm, instead for fractal WPM it is about 1 μm.

Thus for soluble WPA, the formation of the shell appears at a larger scale. The shell itself exhibits a gradient of elasticity because the Darcy pressure increases from the inner part of the shell to the outer part. A larger shell is more likely to have an uneven density. As explained above, such shells may be able to sustain more compression in their inner part than in its outer part, leading to a shrivelled particle shape. In case of smaller characteristic length, colloidal particles accumulate in a thinner shell, which may collapse more uniformly, inducing a simple folding instability leading to a cup-like shape. This folding to shrivelling transition has been detailed precisely in some model cases [34]. Obviously, the mechanisms suggested here require further studies to be confirmed. But the delicate mechanical properties of the gel-like network of proteins, particularly the behaviour under compression, in addition to the presence of a gradient of density make a precise modelling of the shells an extremely difficult challenge.

Conclusion

This paper shows the rationalization of morphology development during drying of single droplets of protein suspensions. Non-aggregated and aggregated whey protein dispersions were used as reference systems, with and without salt addition. Morphology development was characterized experimentally by evaluating the evaporation rate, as well as the locking and buckling times, both by macro and microscopy. Results showed no significant difference in terms of evaporation rate, locking and buckling time among the colloidal dispersions and as a function of salt addition. However, a significant characteristic final morphology was observed. Specifically, particle changed from shriveled to cup-like shape at increasing colloidal sizes. Estimation of physical parameters affecting shell formation and mechanical properties anticipated a buckled/shriveled morphology of dry droplets as in agreement to experimental observations. The formation of a solid shell at the particle surface was predicted. In addition, calculation of the DLVO potential showed that colloidal interaction were dominated by van der Waals attraction. Hence, the diverse final morphology was explained by assuming the formation of elastic layers at the particle surface with different compression stress.

Finally, this work showed that it is possible to achieve diverse final morphology of particles using same drying conditions and starting from the same type of colloids (WPI) but with different degree of aggregation. In addition, it is possible to predict the final morphology of particle by estimating mechanical properties of the particle shell. This evidence of applicability of fundamental knowledge, in terms of the modelling of the colloidal aspects of dispersion dying, establishes a first base for controlling particle formation as well as functionality of food and pharma protein products on a dry state.

Acknowledgement

This project has received funding from the European Union's Horizon 2020 research and innovation program under the Marie Sklodowska-Curie grant agreement No 706061. The authors would like to thank Gene Lam and Socrates Foschini for technical assistance during SEM microscopy; ScopeM (ETH Zurich) for offering SEM measurement time; Prof R. Mezzenga and his group (FSM Laboratory at ETH Zurich) for offering Malvern Z sizer measurement time.

References

[1] J. Bouman, P. Venema, R. J. de Vries, E. van der Linden, and M. A. I. Schutyser, "Hole and vacuole formation during drying of sessile whey protein droplets," *Food Res. Int.*, vol. 84, pp. 128–135, 2016.

[2] E. M. Both, A. M. Karlina, R. M. Boom, and M. A. I. Schutyser, "Morphology development during sessile single droplet drying of mixed maltodextrin and whey protein solutions," *Food Hydrocoll.*, vol. 75, pp. 202–210, 2018.

[3] C. Schmidmeier, C. O'Gorman, K. Drapala, D. Waldron, J. O'Mahony, Elucidation of factors responsible for formation of white flecks in reconstituted fat filled milk powders, Colloids and Surfaces A: Physicochemical and Engineering Aspects, 2019 vol: 575 pp: 245-255

[4] A. Sharma, A. H. Jana, R. S. Chavan, Functionality of Milk Powders and Milk-Based Powders for End Use Applications—A Review. Comprehensive Reviews in Food Science and Food Safety, 2012, Vol 11, pp: 518-528

[5] G. Ronse *et al.*, "Microstructure evolution of micellar casein powder upon ageing: Consequences on rehydration dynamics," *J. Food Eng.*, vol. 206, pp. 57–66, 2017.

[6] J. Ji, K. Cronin, J. Fitzpatrick, and S. Miao, "Enhanced wetting behaviours of whey protein isolate powder: The different effects of lecithin addition by fluidised bed agglomeration and coating processes," *Food Hydrocoll.*, vol. 71, pp. 94–101, 2017.

[7] S. V. Crowley, B. Desautel, I. Gazi, A. L. Kelly, T. Huppertz, J. A. O' Mahony, Rehydration characteristics of milk protein concentrate powders, Journal of Food Engineering, 2015, vol. 149, pp. 05-113.

[8] C. Sadek, H. Li, P. Schuck, Y. Fallourd, N. Pradeau, C. Le Floch-Fouéré, R. Jeantet, "To What Extent Do Whey and Casein Micelle Proteins Influence the Morphology and Properties of the Resulting Powder?," *Dry. Technol.*, vol. 32, no. 13, pp. 1540–1551, 2014.

[9] L. Lanotte, F. Boissel, P. Schuck, R. Jeantet, C. Le Floch-Fouéré, Drying-induced mechanisms of skin formation in mixtures of high protein dairy powders, Colloids and Surfaces A: Physicochemical and Engineering Aspects, 2018 vol: 553 pp: 20-27

[10] Y. Fang, S. Rogers, C. Selomulya, and X. D. Chen, "Functionality of milk protein concentrate: Effect of spray drying temperature," *Biochem. Eng. J.*, vol. 62, pp. 101–105, 2012.

[11] E. Panagopoulou, V. Evageliou, N. Kopsahelis, D. Ladakis, A. Koutinas, I. Mandala, Stability of double emulsions with PGPR, bacterial cellulose and whey protein isolate, Colloids and Surfaces A: Physicochemical and Engineering Aspects, 2017, vol. 522, pp.445-452.

[12] J. K. Keppler, K. Schwarz, Increasing the emulsifying capacity of whey proteins at acidic pH values through covalent modification with allyl isothiocyanate, Colloids and Surfaces A: Physicochemical and Engineering Aspects, 2017, vol 522, pp. 514-524.

[13] M. Chevallier, A. Riaublanc, C. Cauty, P. Hamon, F. Rousseau, J. Thevenot, C. Lopez, T. Croguennec, The repartition of whey protein microgels and caseins between fat droplet surface and the continuous phase governs the heat stability of emulsions, Colloids and Surfaces A: Physicochemical and Engineering Aspects, 2019, vol. 563, pp. 217-225

[14] E. Lintingre, F. Lequeux, L. Talini, and N. Tsapis, "Control of particle morphology in the spray drying of colloidal suspensions," *Soft Matter*, vol. 12, no. 36. pp. 7435–7444, 2016.

[15] G. Gauthier, V. Lazarus, L. Pauchard, Alternating Crack Propagation during Directional Drying, Langmuir, 2007, vol 23 (9), pp. 4715-4718

[16] G. W. Scherer, “Recent progress in drying of gels,” *J. Non. Cryst. Solids*, vol. 147–148, no. C, pp. 363–374, 1992.

[17] P. Atkins and J. de Paula, “Atkins’s physical chemistry.” Oxford University Press, 2006.

[18] C. Schmitt, C. Bovay, A.-M. Vuilliomenet, M. Rouvet and L. Bovetto, “Influence of protein and mineral composition of whey protein isolates on the formation of microgels upon heat treatment," *Food Hydrocoll.*, vol. 25, no. 4, pp. 558-567, 2011.

[19] T. Phan-Xuan, D. Durand, T. Nicolai, L. Donato, C. Schmitt and L. Bovetto, “On the crucial importance of the pH for the formation and self-stabilisation of protein microgels and strands," *Langmuir*, vol. 27, no. 24, pp. 15092-15101, 2011.

[20] G. Unterhaslberger, C. Schmitt, C. Sanchez, C. Appolonia-Nouzille, and A. Raemy, “Heat denaturation and aggregation of β-lactoglobulin enriched WPI in the presence of arginine HCl, NaCl and guanidinium HCl at pH 4.0 and 7.0,” *Food Hydrocoll.*, vol. 20, no. 7, pp. 1006–1019, 2006.

[21] S. W. Provencher and P. Štěpánek, “Global analysis of dynamic light scattering autocorrelation functions,” *Part. Part. Syst. Charact.*, vol. 13, no. 5, pp. 291–294, 1996.

[22] K. Kolwas, G. Derkachov, M. Zientara, M. Kolwas, and D. Jakubczyk, “Evaporation of Micro-Droplets: the ‘Radius-Square-Law’ Revisited,” *Acta Phys. Pol. A*, vol. 122, no. 4, pp. 709–716, 2016.

[23] K. N. Ryan, B. Vardhanabhuti, D. P. Jaramillo, J. H. van Zanten, J. N. Coupland, and E. A. Foegeding, “Stability and mechanism of whey protein soluble aggregates thermally treated with salts,” *Food Hydrocoll.*, vol. 27, no. 2, pp. 411–420, 2012.

[24] C. Schmitt *et al.*, “Internal structure and colloidal behaviour of covalent whey protein microgels obtained by heat treatment,” *Soft Matter*, vol. 6, no. 19, pp. 4876–4884, 2010.

[25] T. Nicolai, M. Britten, and C. Schmitt, “β-Lactoglobulin and WPI aggregates: Formation, structure and applications,” *Food Hydrocoll.*, vol. 25, no. 8, pp. 1945–1962, 2011.

[26] T. Nicolai, D. Durand, A. Riaublanc, N. Mahmoudi, and S. Mehalebi, “Light-Scattering Study of the Structure of Aggregates and Gels Formed by Heat-Denatured Whey Protein Isolate and β-Lactoglobulin at Neutral pH,” *J. Agric. Food Chem.*, vol. 55, no. 8, pp. 3104–3111, 2007.

[27] S. Mehalebi, T. Nicolai, and D. Durand, “Light scattering study of heat-denatured globular protein aggregates,” *Int. J. Biol. Macromol.*, vol. 43, no. 2, pp. 129–135, 2008.

[28] J. M. Aguilera and P. Baffico, “Structure-mechanical properties of heat-induced whey protein/cassava starch gels,” *J. Food Sci.*, vol. 62, no. 5, 1997.

[29] D. A. Weitz *et al.*, “Onset of Buckling in Drying Droplets of Colloidal Suspensions,” *Phys. Rev. Lett.*, vol. 94, no. 1, 2005.

[30] C. Schmitt, C. Bovay, M. Rouvet, S. Shojaei-Rami, and E. Kolodziejczyk, “Whey protein soluble 348 aggregates from heating with NaCl: Physicochemical, interfacial, and foaming properties,” 349 Langmuir, vol. 23, no. 8, pp. 4155–4166, 2007.

[31] S. Torquato, T. M. Truskett, and P. G. Debenedetti, “Is random close packing of spheres well defined?,” *Phys. Rev. Lett.*, vol. 84, no. 10, pp. 2064–2067, 2000.

[32] R. Vehring, “Pharmaceutical particle engineering via spray drying,” *Pharm. Res.*, vol. 25, no. 5, pp. 999–1022, 2008.

[33] A. Bouchoux, P. Qu, P. Bacchin, and G. Gésan-Guiziou, “A general approach for predicting the filtration of soft and permeable colloids: The milk example,” *Langmuir*, vol. 30, no. 1, pp. 22–34, 2014.

[34] F. Brau, P. Damman, H. Diamant, and T. A. Witten, “Wrinkle to fold transition: Influence of the substrate response,” *Soft Matter*, vol. 9, no. 34. pp. 8177–8186, 2013.

Revised Table(s)

Table 1. Composition and pH of colloidal dispersions

Whey protein aggregates	Solid content of WPI dispersions (wt%)	pH-adjustment
Whey protein microgels (WPM)	4.0	5.9
Fractal WPM	7.0	5.9
Soluble whey protein aggregates (WPA)	7.0	6.9

Table 2. Hydrodynamic diameter and polydispersity of colloidal dispersions

Colloidal dispersions	Added NaCl [wt% db]	Hydrodynamic diameter [nm]		Polydispersity index	
		Average	SD*	Average	SD*
Filtered WPI	0	11.73	0.05	0.52	0.002
WPI	0	182	2.89	0.32	0.026
Soluble WPA	0	49.2	0.23	0.28	0.021
	1	49.5	0.88	0.29	0.019
	3	54.9	0.75	0.34	0.016
	6	49.2	0.42	0.28	0.015
WPM	0	230	3.00	0.18	0.021
	1	229	0.47	0.19	0.006
	3	229	1.28	0.17	0.016
	6	227	1.35	0.17	0.008
Fractal WPM	0	291	6.89	0.35	0.026
	1	290	4.31	0.34	0.035
	3	293	2.65	0.35	0.040
	6	289	1.4	0.36	0.008

**SD = standard deviation*

Revised Figure(s)

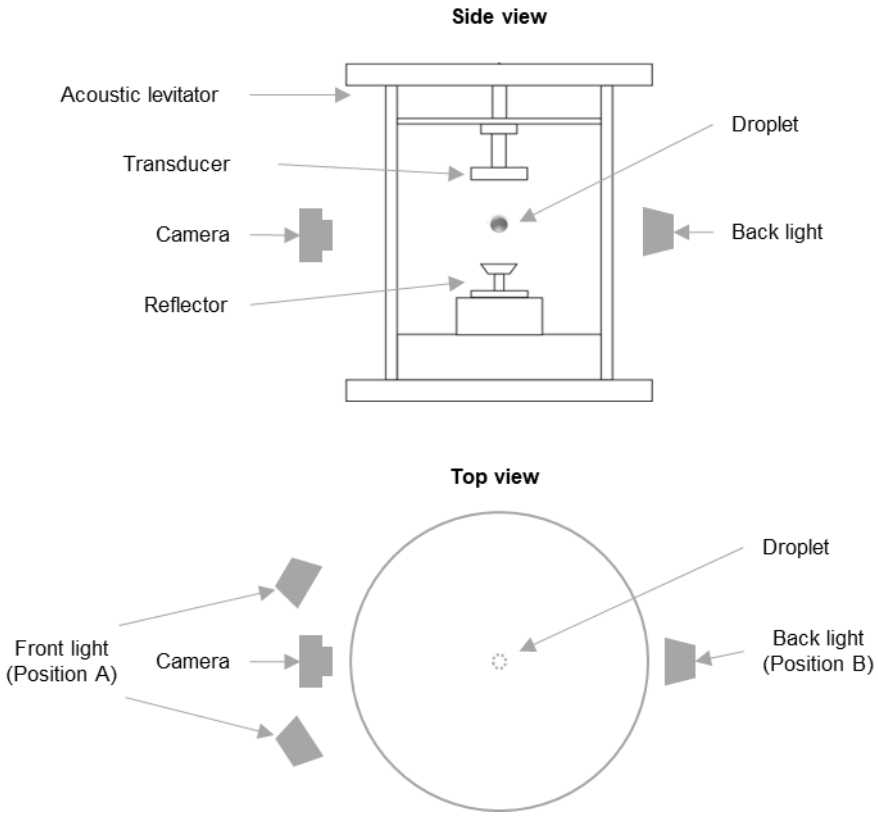

Figure 1. Sketch of the single-drop drying-kinetics device

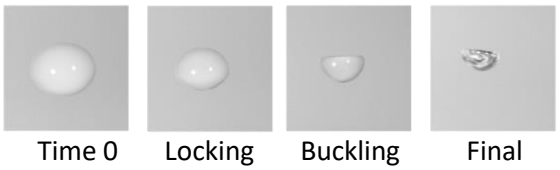

Figure 2. Example images corresponding to characteristic times of morphology development of a single droplet

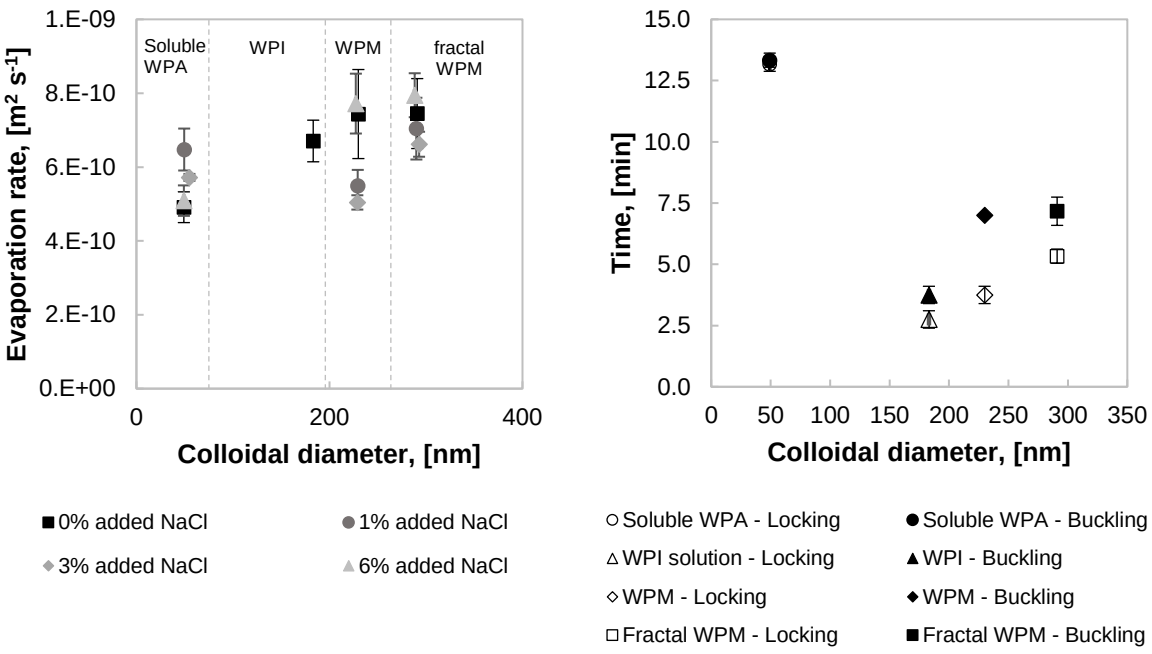

Figure 3. Evaporation rate as a function of colloidal diameter and NaCl addition for soluble WPA, WPI, WPM and fractal WPM droplets (left). Locking and Buckling times as a function of colloidal diameter for soluble WPA, WPI, WPM and fractal WPM droplets (right).

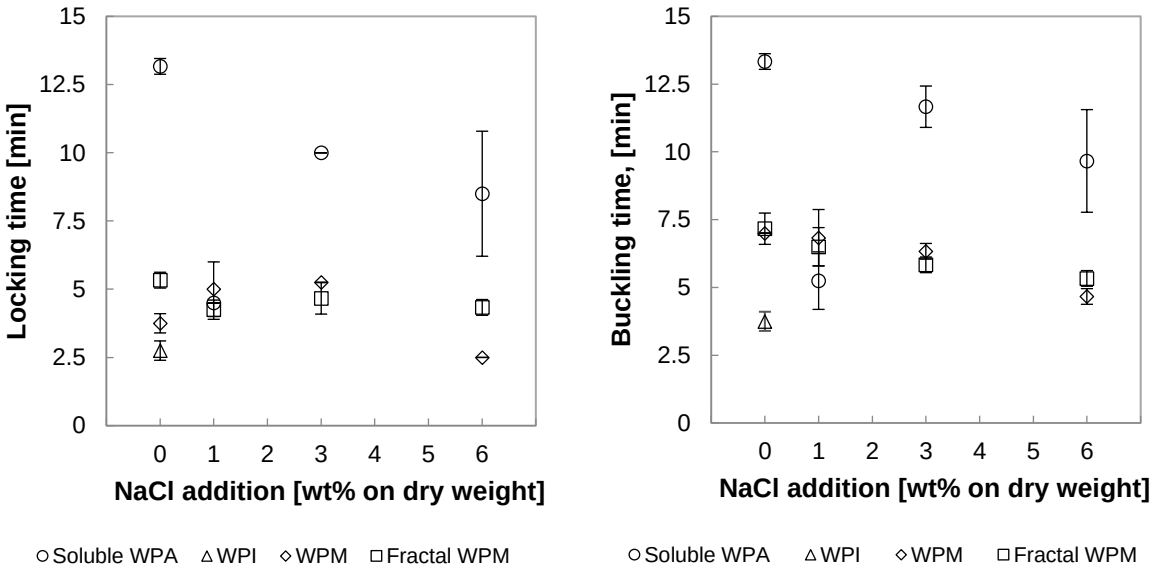

Figure 4. Locking time (left) and buckling time (right) as a function of NaCl addition for soluble WPA, WPI, WPM and fractal WPM droplets.

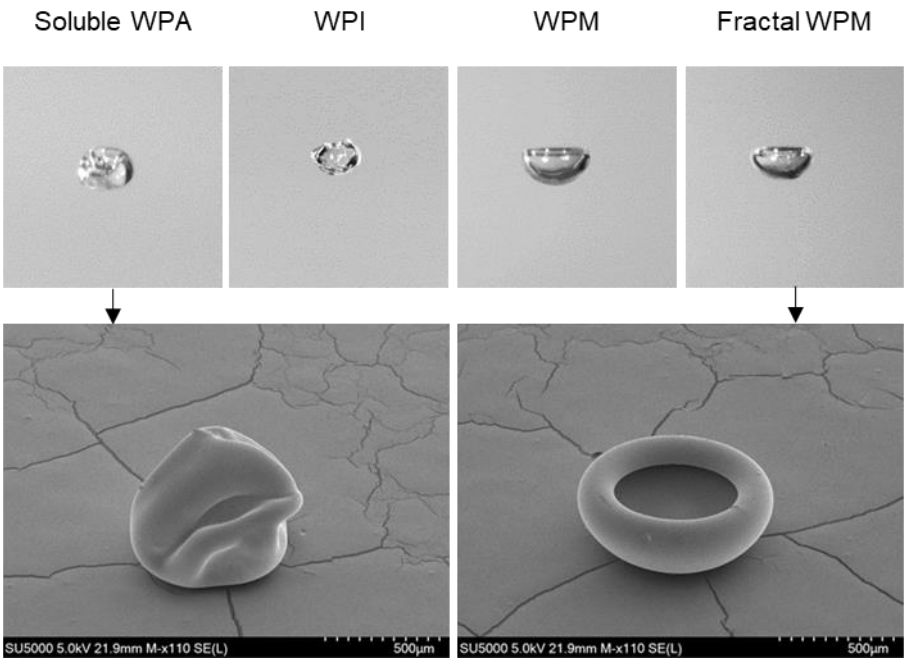

Figure 5. Top pictures: final morphology of soluble WPA, WPI, WPM and fractal WPM droplets captured using a macro camera. Bottom pictures: final morphology of soluble WPA (left) and fractal WPM (right) observed by SEM.

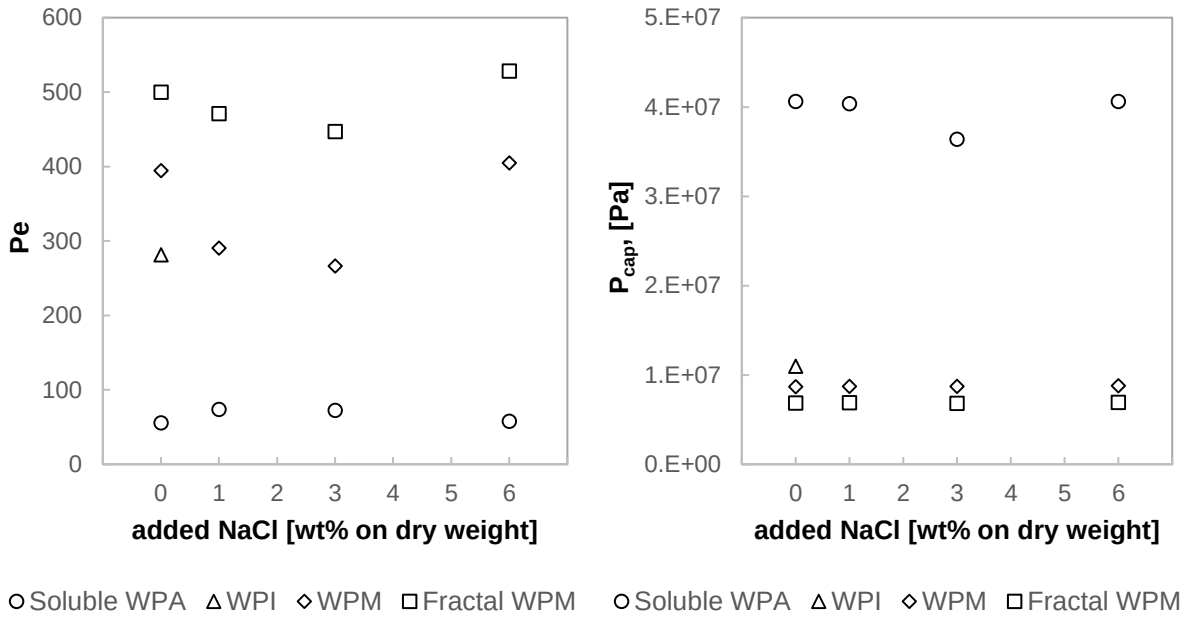

Figure 6. Péclet dimensionless number (left) and Capillary pressure (right) as a function of NaCl addition for soluble WPA, WPI, WPM and fractal WPM droplets.

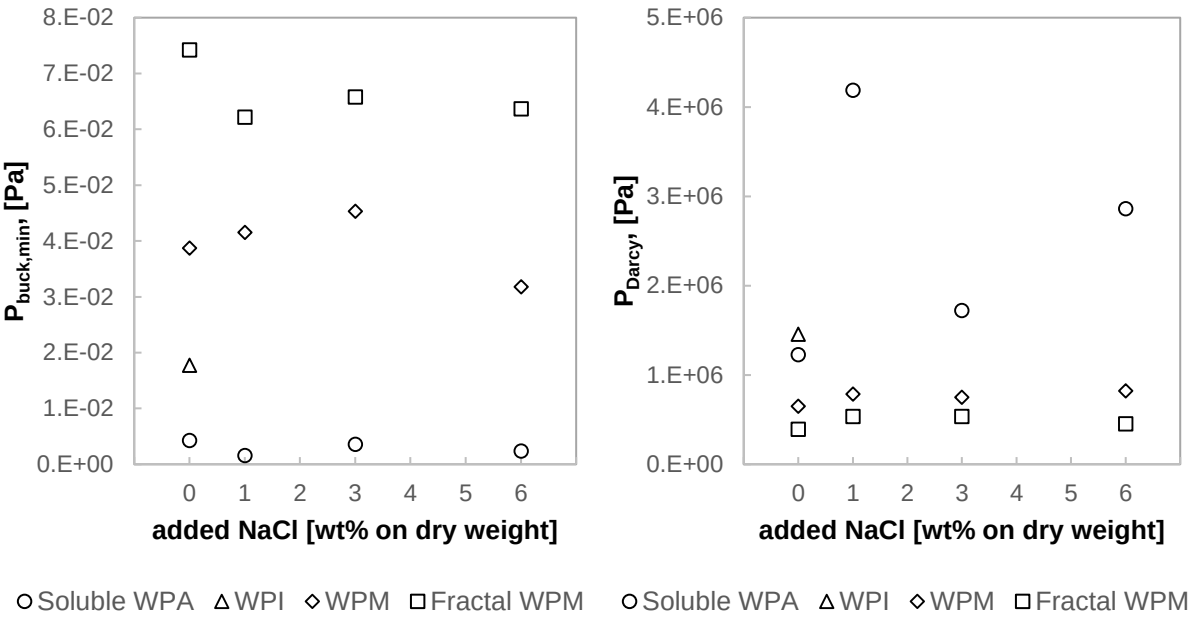

Figure 7. Minimum buckling pressure (left) and Darcy's pressure (right) as a function of NaCl addition for soluble WPA, WPI, WPM and fractal WPM droplets.